Volume 39 | Number 4 | April 2015 | Pages 2351–3152

NJC

New Journal of Chemistry

A journal for new directions in chemistry

www.rsc.org/njc

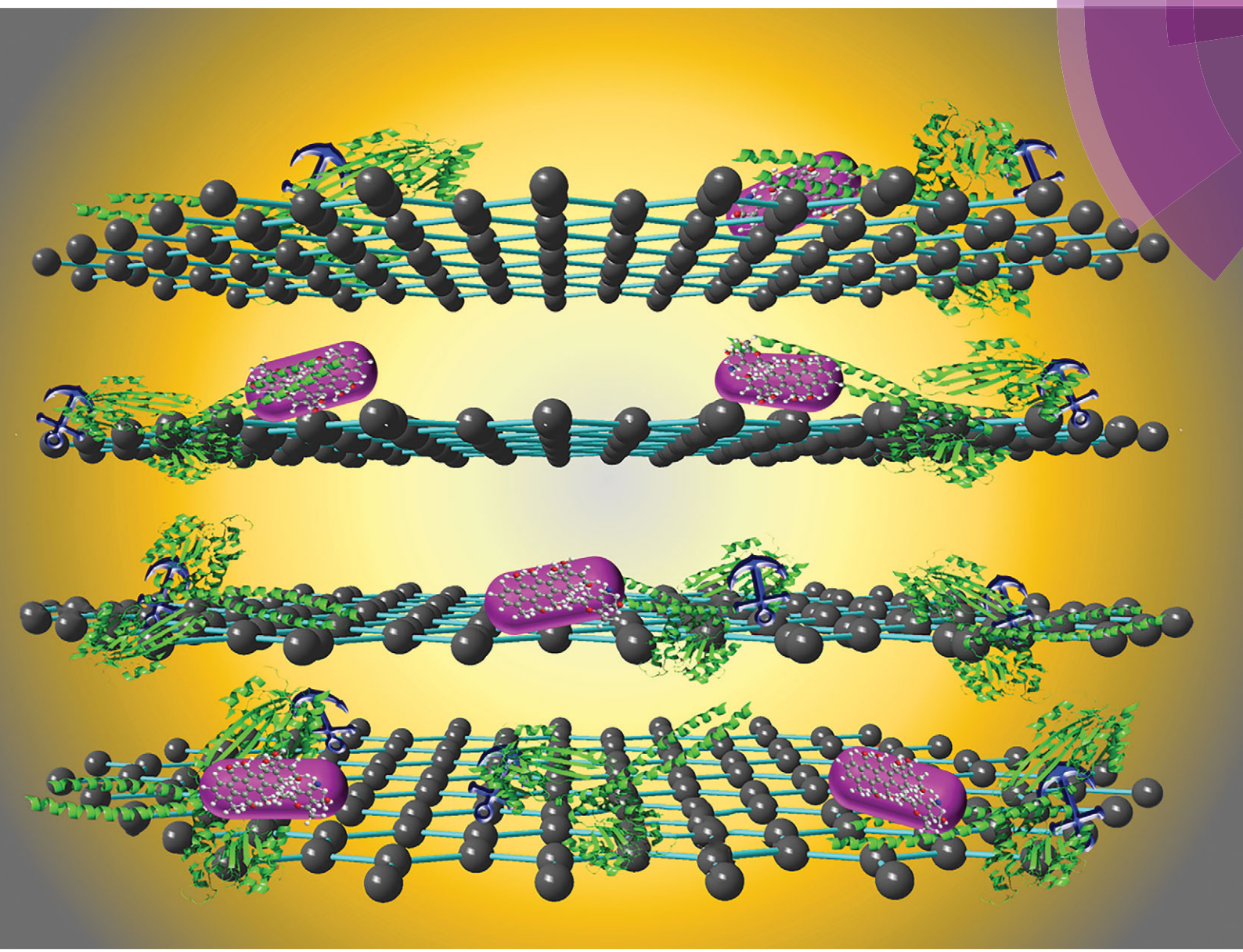

ISSN 1144-0546

ROYAL SOCIETY OF CHEMISTRY

PAPER

Goutam De, Arnab Mukherjee *et al.*

Synthesis of amine functionalized graphite nanosheets and their water-soluble derivative for drug loading and controlled release

cnrs

NJC

PAPER

View Article Online
View Journal | View Issue

Cite this: *New J. Chem.*, 2015, 39, 2451

Synthesis of amine functionalized graphite nanosheets and their water-soluble derivative for drug loading and controlled release†

Amrita Chakravarty, Koushik Bhowmik, Goutam De* and Arnab Mukherjee*

Received (in Montpellier, France) 10th September 2014,
Accepted 8th December 2014

DOI: 10.1039/c4nj01545b

www.rsc.org/njc

A facile route to synthesize amine ($-NH_2$) functionalized graphite nanosheets (AFGNS) by 2-step controlled chemical modification of microcrystalline graphite is described. The method begins with nitration by mixed acid ($HNO_3 : H_2SO_4$ in 1 : 1 v/v ratio), followed by reduction with Na_2S to form AFGNS. The AFGNS was reacted with carboxylic acid-terminated polyethylene glycol (PEG) chains (MeO–mPEG–COOH, M_W = 5000 Da) in the presence of a carbodiimide coupling agent to obtain a water-soluble PEGylated AFGNS (P-AFGNS) composite. Anticancer drug doxorubicin (DOX) was loaded on this composite with a loading capacity of 0.296 mg mg^{-1} for an initial concentration of 0.232 mg mL^{-1} DOX and 0.136 mg mL^{-1} of P-AFGNS and the release of DOX from this water-soluble DOX loaded P-AFGNS composite at two different temperatures was found to be strongly pH dependent.

Introduction

The recent applications of graphite nanosheets (GNS) in biological systems, energy storage and catalysis[1–5] have attracted much attention in the development of efficient, scalable routes to this material owing to its highly conjugated sp^2 hybridized system with lateral dimensions less than 100 nm.[6] However, a major impediment that hinders their application in the preparation of the functional materials as well as in biological systems is their inherent insolubility in different organic–aqueous solvents. Covalent chemical functionalization of GNS potentially overcomes these issues by creating functional groups on the surface of the nanosheet, which not only increases its dispersibility in various organic solvents[7,8] but also creates a band gap for applications in photonics and microelectronics.[9] In the case of biological applications, the primary requirement for GNS sample preparation is its dispersibility in water, biocompatibility and nontoxicity.

Graphene oxide (GO), the highly oxygen rich chemically modified derivative of graphite has very high dispersibility in water, and has been explored for several biomedical applications like drug delivery, controlled loading/release of antitumor agents and biosensors.[10–15] However, recent developments in GO reveal its cytotoxic nature that directly interferes with the electron transport chain accelerating the formation of reactive oxygen species which have a severe damaging effect on DNA and amino acids, leading to the aggregation of human platelets *in vivo* and induced apoptosis.[16–19] Further, in the case of mice, it was observed that administering GO intravenously into their body causes extensive pulmonary thromboembolism.[19] The applications of GO in the field of biomedical sciences is thus no longer favoured. Thus, the synthesis of an alternative functional group, which is cytocompatible and will lead to increased dispersibility of GNS in aqueous as well as organic medium, is imperative. The amine ($-NH_2$) group was found to be cytoprotective in nature.[20] It also increases the dispersibility of graphene sheets in solvents.[21] Recently, $-NH_2$ functionalized graphene was reported to be more biocompatible than GO for biomedical applications.[20,22–24]

Synthesis of $-NH_2$ functionalized graphene was primarily carried out either by direct ion implantation of the $-NH_2$ group,[22,23] N-doping of graphene by ammonia plasma,[25] covalent attachment of bifunctional cross linkers with GO[24,26] or by 1,3 dipolar cycloaddition on to the graphene surface.[27] Similarly in the case of graphite, the $-NH_2$ group was fabricated by vacuum ultraviolet induced photochemistry in the presence of ammonia,[28] by treatment with ammonia plasma[29] or by ultrasonic treatment with triethylenetetramine and ammonium carbonate.[30] However, some of the above mentioned methods are expensive owing to their instrumental set up and require extreme precaution as

CSIR-Central Glass & Ceramic Research Institute, 196, Raja S. C. Mullick Road, Kolkata-700032, West Bengal, India. E-mail: gde@cgcri.res.in, arnabm@cgcri.res.in; Fax: +91-33-24730957

† Electronic supplementary information (ESI) available: FTIR spectra, TGA analysis and XPS survey scan of microcrystalline graphite, NFGNS and AFGNS; high resolution N1s spectra of NFGNS and AFGNS; a zeta potential plot of AFGNS dispersion as a function of pH; a digital photograph of aqueous dispersion of AFGNS; centrifugates of P-AFGNS, AFGNS and graphite; Raman spectra of P-AFGNS and AFGNS; TEM and HRTEM of P-AFGNS; an AFM image of P-AFGNS; FESEM of AFGNS and P-AFGNS; calibration curve of DOX and UV-Vis spectra for DOX loading in AFGNS and P-AFGNS. See DOI: 10.1039/c4nj01545b

several sensitive parameters have to be maintained during the process of functionalization. Therefore, a simple wet chemical process for the direct attachment of the $-NH_2$ group on to the surface of GNS is considered to be a cheap, easy and viable option. To the best of our knowledge, no such process has been reported yet.

In this study, we report the synthesis of amine ($-NH_2$) functionalized GNS (AFGNS) from microcrystalline graphite by two simple steps of controlled chemical functionalization. The process includes nitration followed by reduction. Since polymer functionalities have been employed earlier to obtain soluble dispersions of graphite, graphene and SWCNT,[10,11,31] the AFGNS obtained was reacted with –COOH terminated polyethylene glycol (PEG) chains, a non-toxic and non-immunogenic polymer,[32] to give a water-soluble PEGylated AFGNS (P-AFGNS) composite. The anticancer drug doxorubicin (DOX) was loaded onto this composite with sufficient loading capacity plausibly by hydrogen bonding and π–π stacking interaction.[33] Release of DOX from the P-AFGNS was found to be pH dependent, which makes it a promising material as a drug carrier for targeted delivery of anticancer drugs.

Experimental procedure

Materials

The following chemicals were used as received: graphite powder (<20 μm, synthetic), MeO–mPEG–COOH (M_W = 5000 Da), doxorubicin hydrochloride, 1-ethyl-3-(3-dimethylaminopropyl) carbodiimide hydrochloride (EDC) and 2-mercaptoethanol were purchased from Sigma Aldrich. Concentrated H_2SO_4 (36 N), concentrated HNO_3 (16 N) and sodium sulphide (Na_2S) were supplied by Merck and a 0.22 μm polyvinylidene fluoride (PVDF) membrane was purchased from Millipore. Water (18 MΩ) was obtained from a Milli-Q System (Millipore).

Characterization

The details of the Raman spectra were obtained using a Renishaw InVia Reflex micro Raman spectrometer with excitation by argon ion (514 nm) laser. The laser power was kept sufficiently low to avoid heating of the samples and the spectra were collected with a resolution of 1 cm^{-1}. Multiple spectra (3–5) were obtained, normalized to the G band, and averaged to present a comprehensive overview of the material. Fourier transform infrared (FT-IR) spectra of the samples were recorded using a Nicolet 380 FT-IR spectrometer. FT-IR data was collected using the KBr pellet method. X-ray photoelectron spectroscopy (XPS) measurements were done on a PHI 5000 Versaprobe II XPS system with a Al Kα source and a charge neutralizer at room temperature, maintaining a base pressure at about 6×10^{-10} mbar and an energy resolution of 0.6 eV. Low resolution survey scans and high resolution scans of C 1s and N 1s were taken. At least two separate locations were analyzed for each sample. UV-Visible absorption spectra of the aqueous solutions containing DOX for monitoring the loading and release of the drug were recorded using a Cary 50, Varian Inc spectrometer. Photoluminescence emission spectra of the aqueous solutions of DOX were recorded using a Photon Technology International QM-30 spectrometer.

Zeta potential of the aqueous dispersion of AFGNS and P-AFGNS (0.125 mg mL^{-1}) were measured using a Nano Particle Analyzer SZ-100, Horiba. TGA data was obtained using a Netzsch TG 209 F3 Tarsus thermal analyzer. Samples were degassed at 80 °C for 15 min and then heated at 10 °C min^{-1} to 700 °C in a N_2 atmosphere and held there for 20 min.

A transmission electron microscope (TEM) and high resolution TEM (HRTEM) images were taken using a JEOL JEM-2100F (FEG) operated at an accelerating voltage of 200 kV. The surface morphology of powder samples were observed from field emission scanning electron microscope (FESEM) images obtained using a ZEISS SUPRA 35 VP FESEM. Atomic force microscopic (AFM) images were recorded using a Multiview 3000 (Nanonics) atomic force microscope. The AFM samples were prepared by spin coating (5000 rpm) diluted ethanolic solutions of the samples (0.05 mg mL^{-1}) on a cleaned one side polished Si wafer (1.5 by 1.5 cm^2).

Synthesis of AFGNS

AFGNS was synthesized *via* two simple steps of chemical modification. The first step involved synthesis of the nitro ($-NO_2$) functionalized GNS (NFGNS). This was carried out by adding 50 mg (4.2 mmol) of microcrystalline graphite powder with 50 mL of mixed acid (HNO_3 (16 N) : H_2SO_4 (36 N) in 1 : 1 v/v ratio) in a dry 250 mL round bottom flask under ambient conditions. The reaction mixture was sonicated for 30 min in an ultrasonic bath and then vigorously stirred for 24 h at room temperature. The solution was then quenched with 500 mL distilled water, filtered through 0.22 μm PVDF membrane and washed thoroughly with water until the filtrate became neutral. The NFGNS powder obtained was dried overnight under vacuum and collected. This was followed by reduction of the $-NO_2$ group to $-NH_2$ group using Na_2S as a reducing agent. In a typical reduction reaction, a 50 mL round bottom flask was charged with 5 mg (0.4 mmol) of NFGNS. This was dispersed in 5 mL of distilled water and sonicated for 45 min in an ultrasonic bath to obtain a stable dispersion. 75 mg of Na_2S was then added to this dispersion and the mixture was refluxed at 160 °C for 24 h. The final product was filtered through a 0.22 μm PVDF membrane and thoroughly washed with 100 mL distilled water in small portions to remove the excess Na_2S and other by-products formed. The AFGNS powder obtained was then dried overnight *in vacuo* and collected.

Synthesis of PEGylated AFGNS (P-AFGNS)

In a typical procedure,[11] 3 mg (0.25 mmol) of AFGNS was dissolved in 5 mL distilled water and sonicated for 30 min to get a homogeneous dispersion. MeO–mPEG–COOH (12.5×10^{-2} mmol) in water (15 mL) was then added to the reaction mixture and sonicated for 15 min. EDC (0.42 g, 2.2 mmol) was added to the solution and the dispersion was sonicated for 60 min followed by stirring under ambient conditions for 12 h. The reaction was terminated by adding 2-mercaptoethanol. The resultant solution was centrifuged at 10 000 rpm for 20 min. The residue was redispersed in distilled water and the centrifugation process was repeated thrice to

remove excess PEG and impurities formed during the reaction. The PEGylated AFGNS (P-AFGNS) thus obtained was dried *in vacuo* and collected.

Loading of DOX on P-AFGNS (P-AFGNS–DOX)

DOX was loaded on to P-AFGNS, following the process reported by Yang *et al.*[34] In a typical process, 0.136 mg mL^{-1} of P-AFGNS in water was sonicated with a DOX solution of initial concentration of 0.232 mg mL^{-1} at neutral pH (pH = 7) for 30 min. This solution was then stirred over night in dark at room temperature. Finally, it was centrifuged at 11 000 rpm for 30 min. The same procedure was also carried out with AFGNS and, subsequently, PEGylation was carried out on DOX-loaded AFGNS (AFGNS–DOX) for the control-experiment.

A calibration curve for DOX was prepared with different known concentrations by optical absorption spectral analysis at 480 nm. This calibration curve was used to determine the concentration of DOX. The DOX loading capacity for an initial concentration of 0.232 mg mL^{-1} of DOX and 0.136 mg mL^{-1} of P-AFGNS was calculated using the following equation[34]

$$\text{Drug loading capacity} = (W_{\text{administered dose}} - W_{\text{residual dose}})/W_{\text{P-AFGNS}}$$

here $W_{\text{administered dose}}$ indicates the initial weight of the drug used for loading, $W_{\text{residual dose}}$ indicates the residual weight of drug remaining in the solution after loading on to P-AFGNS and $W_{\text{P-AFGNS}}$ indicates the weight of P-AFGNS used for loading the drug. Drug loading capacity was also studied for AFGNS–DOX in a similar manner. The DOX loaded P-AFGNS composite was named P-AFGNS–DOX.

The drug release behaviour of P-AFGNS–DOX was monitored *in vitro* by dispersing the powder in phosphate buffer saline (PBS, pH 5.5 and 7.4 adjusted with phosphoric acid) under constant stirring at 25 and 37 °C. The DOX dissolved supernatant solution was collected at different time intervals and analysed using UV-Vis spectroscopy at 480 nm wavelength. The photoluminescence emission spectra of the supernatant solutions were also collected after 72 h.

Results and discussion

Fig. 1 shows the schematic representation of the two-step chemical functionalization and attachment of the $-NH_2$ group on the GNS surface with subsequent PEGylation and loading of DOX. The process begins with the treatment of microcrystalline graphite with mixed acid (HNO_3 (16 N) : H_2SO_4 (36 N) in 1 : 1 v/v ratio) under ambient conditions. The reaction was also carried out with 2 : 1, 1 : 2 and 1 : 3 v/v ratios of HNO_3 and H_2SO_4 respectively. The FTIR spectra of the products formed in all the above mentioned cases are given in Fig. S1, ESI.† The 1 : 1 ratio was found to be specific for the nitration of aromatic compounds in the absence of water (Fig. S1, ESI†).[35,36] Thus, treatment with HNO_3 : H_2SO_4 in a 1 : 1 v/v ratio leads to the formation of the $-NO_2$ group on the surface as well as in between the graphitic layers.[37,38] The concomitant ultrasonication and intercalation of the $-NO_2$ group in functionalized graphite leads to the formation of NFGNS.[39,40] Na_2S has

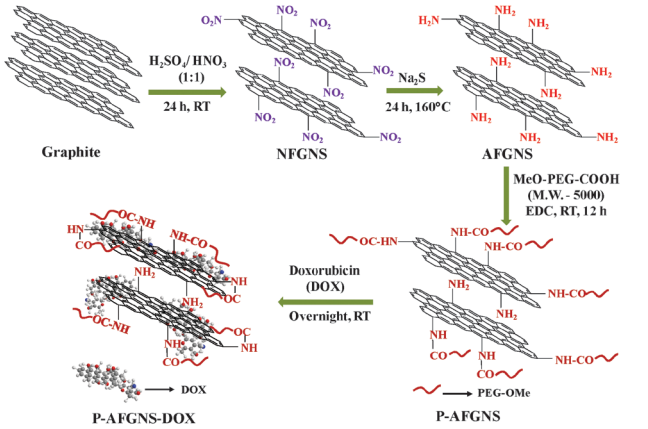

Fig. 1 Schematic diagram showing the two-step controlled synthesis of AFGNS *via* nitration followed by PEGylation of AFGNS to prepare water-soluble P-AFGNS and subsequently loading of DOX to obtain P-AFGNS–DOX.

been previously used for the reduction of aliphatic and aromatic nitro compounds to amine.[41–43] Therefore, treatment of NFGNS with Na_2S in aqueous medium at elevated temperature leads to the reduction of $-NO_2$ groups to $-NH_2$. The reactions occurring may be summed up as follows:

$$HNO_3 + H_2SO_4 \rightarrow NO_2^+ + H_2O^+ + HSO_4^- \quad (1)$$

$$\text{Graphite} + NO_2^+ \rightarrow \text{Graphite–}NO_2\ (\text{NFGNS}) + H^+ \quad (2)$$

$$\text{Graphite–}NO_2 + S^{2-} + H_2O \rightarrow \text{Graphite–}NH_2\ (\text{AFGNS}) + S_2O_3^{2-} + OH^- \quad (3)$$

Subsequently, PEGylation of AFGNS through amide bond formation in the presence of a carbidiimide coupling agent EDC, was performed to form a water-soluble P-AFGNS composite.

$$\text{Graphite–}NH_2 + \text{HOOC–mPEG–OMe} \rightarrow \text{Graphite–NH–CO–mPEG–OMe (P-AFGNS)} \quad (4)$$

Finally, DOX was loaded on P-AFGNS by stirring overnight as shown in Fig. 1.

The derivatized GNS were characterized by Raman, TGA, FT-IR and XPS analysis. Evidence of covalent functionalization can be obtained by inspection of the Raman spectra. As shown in Fig. 2(a), Raman spectra of microcrystalline graphite show a tangential mode (G band) at 1590 cm^{-1} and a weak disorder band (D band) at 1354 cm^{-1} that arises due to the presence of minor defects formed either during the synthesis or at the time of purification of graphite. The D/G ratio was found to be 0.08 for unfunctionalized graphite. However, after functionalization, the D/G ratio of NFGNS increases to ~0.4 (5 times) and the value remained unaltered upon reduction in the case of AFGNS. This confirms the secondary reduction reaction of $-NO_2$ to $-NH_2$ on the GNS surface without any further damage. Moreover, the low D/G value obtained in this case confirms controlled functionalization with much less damage to the conjugated sp^2 hybridized framework of graphite, unlike some other functionalization techniques (like formation of GO) where extensive damage to the graphitic network

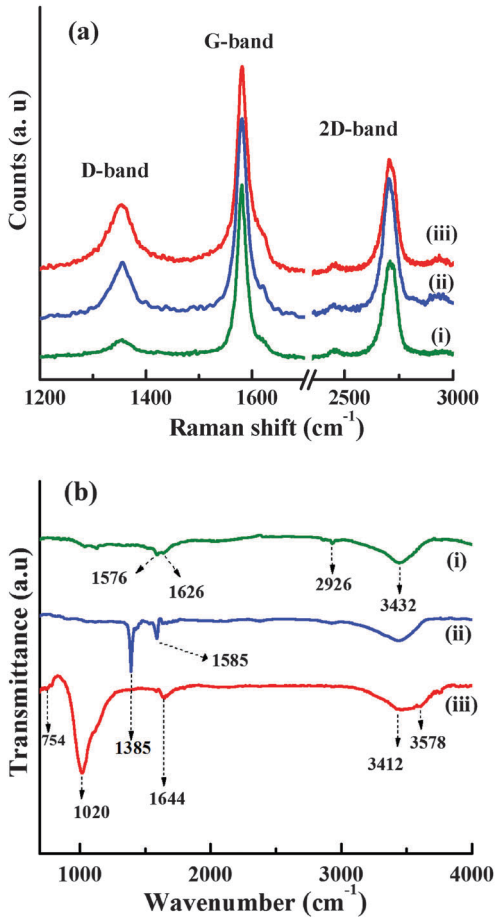

Fig. 2 (a) Raman and (b) FTIR spectra of (i) microcrystalline graphite (ii) NFGNS and (iii) AFGNS.

has been reported.[44] The carbon to functional group ratio was determined by TGA experiments performed under an inert atmosphere on the basis of the weight loss of degassed samples (Fig. S2, ESI†). For microcrystalline graphite, a weight loss of 1.8% was observed, which increased significantly up to 11.4% for NFGNS and 6.7% for AFGNS over the same temperature range of 200 to 350 °C meant for covalent detachment of functional groups.[45] These results were found to be in good agreement with the Raman spectra (Fig. 2a), confirming that approximately 1 out of every 40 carbon atoms were functionalized during the course of the reaction as calculated from the weight loss in TGA.

Fig. 2b shows FT-IR spectra of microcrystalline graphite, NFGNS and AFGNS. Before functionalization, microcrystalline graphite shows peaks at 1576 and 2926 cm^{-1} corresponding to C–C and C–H vibrations of graphitic domains.[46] The peaks observed at 1626 and 3432 cm^{-1} can be attributed to the ambient atmospheric moisture bound to the surface of graphite. After nitration, FT-IR spectra of NFGNS shows a sharp peak at 1385 cm^{-1} along with a small peak at 1585 cm^{-1} due to the N–O stretching frequency of the $-NO_2$ group.[47] However, after amination, the peaks at 1385 and 1585 cm^{-1} disappear along with concomitant appearance of peaks at 754, 1020 and 1644 cm^{-1} that can be attributed to the out of plane N–H bending, C–N stretching and in plane N–H bending of the $-NH_2$ group, respectively.[48,49] The broad band at 3412 cm^{-1} along with a shoulder at 3578 cm^{-1} are due to the presence of N–H stretching frequency of the $-NH_2$ groups.[46,49] Thus, the FT-IR data confirms the reduction of the $-NO_2$ group to $-NH_2$ functionality in AFGNS.

XPS analysis provided direct evidence for the covalent linkage of nitrogen on to the GNS surface during the reaction. XPS spectra of the region corresponding to 0–1100 eV for microcrystalline graphite, NFGNS and AFGNS are shown in ESI† (Fig. S3). The relative atomic percentages are based on the averaged peak areas of two different spots in the same sample and calculated using sensitivity factors 1.0, 1.59 and 2.33 for carbon, nitrogen and oxygen, respectively. XPS survey scans of microcrystalline graphite (Fig. S3a, ESI†), shows the presence of carbon and oxygen whereas in the case of NFGNS and AFGNS (Fig. S3b and c; ESI†), nitrogen is also seen. The relative atomic weight percentage of C and O for graphite was found to be 91.5% and 8.5%, respectively, with no traces of nitrogen. However, in NFGNS and AFGNS, the relative atomic weight percent values for N were found to be 3.7% and 10.5%, respectively, confirming the derivatization of the GNS with nitrogen containing functional groups.[50] It is noteworthy to mention here that while calculating the atomic weight percent values for *N*, the weight % of oxygen and carbon were also taken into consideration. Reduction in the weight % of oxygen on reduction of $-NO_2$ to $-NH_2$ leads to an increase in the relative atomic weight% of *N* in AFGNS.

The high resolution C1s XPS spectrum of microcrystalline graphite on deconvolution by Voigt function[51] shows four different binding energies as shown in Fig. 3a. Peaks with binding energy values at 284.6, 285.1, 286.6 and 290.5 eV corresponds to C=C, C–C, C–O (from atmospheric moisture) and π–π^* interaction for C–C bond shake up respectively.[51,52] However, for C1s spectra of NFGNS (Fig. 3b), along with the peaks at 284.6, 285 and 286.6 eV, a prominent peak at 285.6 eV corresponding to the C–N bond was also observed,[48–50] providing direct evidence for the attachment of the nitrogen containing $-NO_2$ group on GNS (NIST XPS database). The high resolution N1s spectrum of NFGNS (Fig. S4a, ESI†) shows a binding energy value of 400 eV corresponding to the nitrogen atoms embedded in GNS with three carbon neighbours,[50,53] along with a peak at 405 eV for the $-NO_2$ group.[54] On the other hand, for AFGNS, the high resolution C 1s spectrum (Fig. 3c) and N 1s spectrum (Fig. S4b; ESI†) depicts a sharp peak at 285.6 and 400.5 eV for the C–N and N–H bonds of the amine group respectively.[48,49] Moreover, the complete disappearance of the peak at 405 eV corresponding to the $-NO_2$ group, in the N 1s spectrum of AFGNS, reconfirms the complete reduction of NFGNS to AFGNS. The zeta potential of AFGNS from pH 2–10 (adjusted with 0.1 M HCl and 0.1 M NaOH) is given in ESI† (Fig. S5). The zeta potential at pH = 7 was positive with the value of 13.3 mV which in turn proves the $-NH_2$ functionalization in AFGNS.[20]

TEM images of the starting graphite and AFGNS are shown in Fig. 4a and b respectively. The size of the starting graphite was found to be greater than 1 μm (Fig. 4a). However for AFGNS, the size was less than 100 nm (~70–80 nm) as shown in Fig. 4b. The TEM image of microcrystalline graphite with the same magnification as that of AFGNS in Fig. 4b has been shown

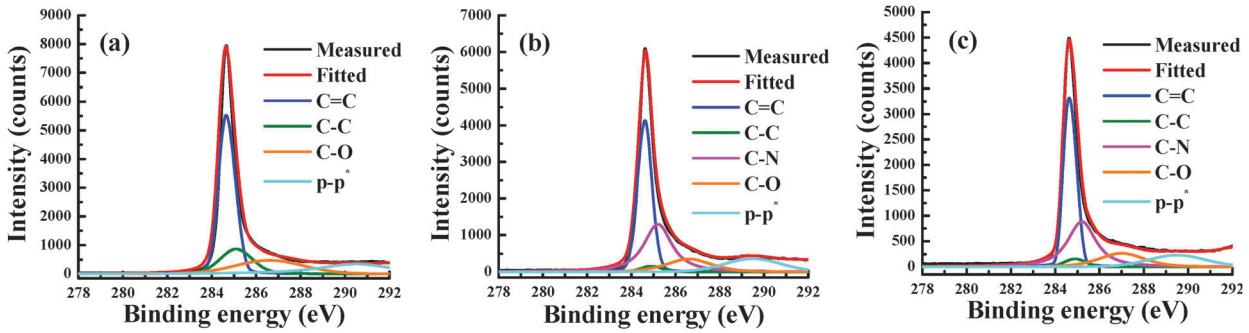

Fig. 3 High resolution C1s XPS spectra of (a) microcrystalline graphite, (b) NFGNS and (c) AFGNS.

in the inset of Fig. 4a. AFM images of AFGNS (Fig. 4e and f) also show a nanosheet having size less than 100 nm, corroborating with the observation from the TEM analysis. The size plays a very crucial role in the potential drug delivery application. It had been observed earlier that GNS with less than 100 nm size can be successfully used for various biomedical applications including drug delivery.[55–58] The HRTEM image of microcrystalline graphite (Fig. 4c) shows smooth edges and sidewalls with visible graphitic lattice fringes having an interlayer spacing of ~3.4 Å.

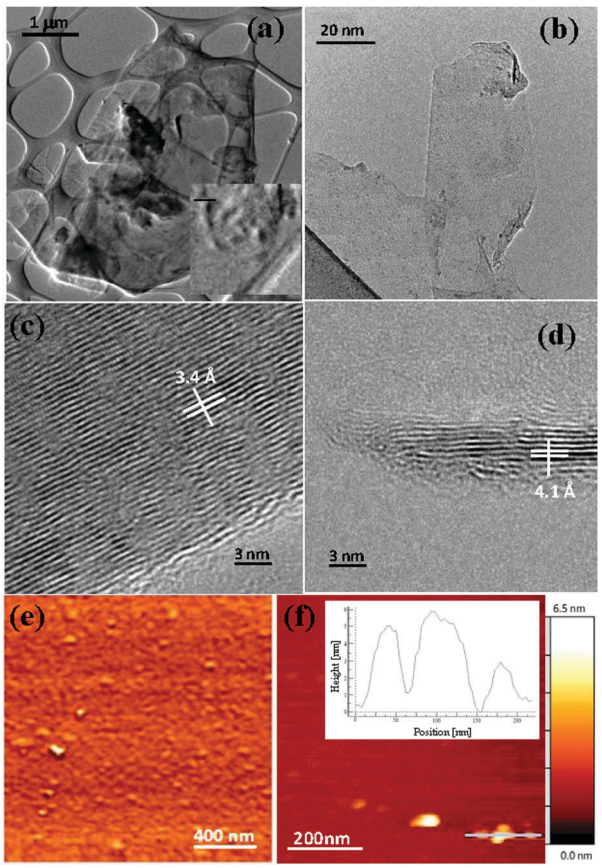

Fig. 4 TEM images of (a) microcrystalline graphite and (b) AFGNS. HRTEM images (c) microcrystalline graphite and (d) AFGNS. The marking for the interlayer spacing has been shown in the images. (e) AFM phase image of AFGNS and (f) height image of AFGNS with the height profile of the marked portion in the inset.

However, an increase in the interlayer spacing to ~4.1 Å due to the intercalated $-NH_2$ groups between the nanosheets was observed in the HRTEM image of AFGNS as shown in Fig. 4d. The thickness of AFGNS was found to be 6 nm as observed from the AFM height profile (inset Fig. 4f) along with thicknesses of 5 and 2.5 nm for adjacent smaller nanosheets indicating the presence of ~6–15 graphitic layers in AFGNS.

The AFGNS formed was found to be highly dispersible in water (Fig. S6; ESI†). But the stability of the dispersion was not very high and the nanosheets settled down after few hours which was also supported by their low zeta potential value (13.3 mV). Thus, AFGNS was further reacted with –COOH terminated PEG chains in the presence of EDC as a coupling agent to give a highly water-soluble, nontoxic GNS composite that has been successfully used for loading the anticancer drug DOX and to study its release profile for potential application in drug delivery. The successful PEGylation of AFGNS was confirmed by FTIR spectra and TGA analysis. The FTIR spectra of P-AFGNS (Fig. 5a) shows a prominent peak at 2926 cm^{-1} followed by peaks at 1100 and 1156 cm^{-1} corresponding to the C–H and C–O stretching of PEG, respectively.[46] Further, significant reduction in the intensity of the peak at 1021 cm^{-1} for the C–N stretching of $-NH_2$ group along with shift in the position of the peak at 1626 cm^{-1} for C═O stretching confirms the formation of –CONH bonds[31] and the attachment of PEG onto the $-NH_2$ group on the AFGNS surface *via* covalent linkage. Due to the co-existence of –OH, the N–H stretching frequencies of amides (−CONH) could not be identified. Appearance of an intense broad peak at 3425 cm^{-1} could be due to overlapping of the N–H of amide and PEG originated –OH stretching frequencies.[46] TGA of microcrystalline graphite, AFGNS and P-AFGNS provides further evidence of the covalent attachment of PEG on AFGNS as shown in Fig. 5b. TGA data for P-AFGNS shows a weight loss of ~30% whereas that for AFGNS was found to be ~15%. The increase in weight loss in the case of P-AFGNS can be attributed to the loss of high molecular weight PEG chains from the AFGNS surface and in turn reconfirms the successful PEGylation of AFGNS.[59] Visual inspection of the supernatant aqueous solution of P-AFGNS, AFGNS and microcrystalline graphite after centrifugation shows a stable dispersion for P-AFGNS (Fig. S7; ESI†) with the zeta potential value of −26.6 mV. Raman spectra of AFGNS and P-AFGNS (Fig. S8; ESI†) exhibit no significant change in the D/G ratio upon attachment of the long PEG chains to the $-NH_2$ groups *via* –CONH bonds.

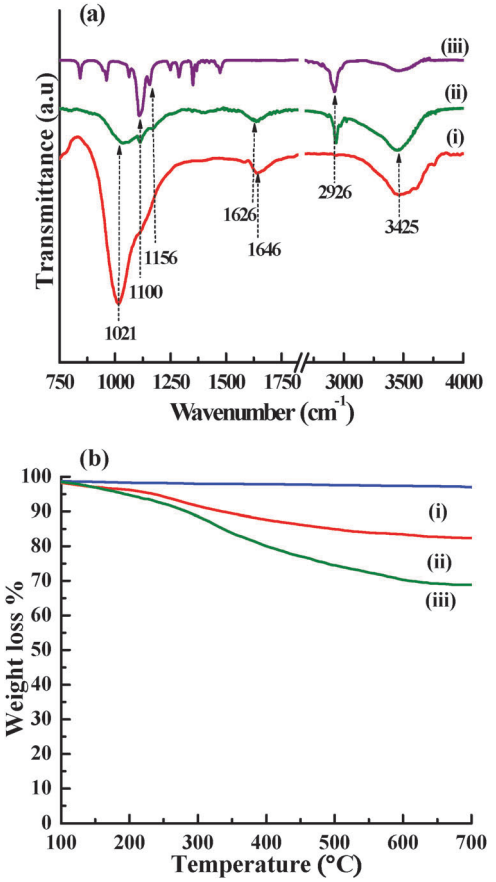

Fig. 5 (a) FTIR spectra of (i) AFGNS, (ii) P-AFGNS and (iii) PEG. (b) TGA graph of (i) microcrystalline graphite, (ii) AFGNS and (iii) P-AFGNS.

TEM and HRTEM image of P-AFGNS (Fig. S9; ESI†) exhibits characteristic roughness pertaining to the attachment of PEG chains on the AFGNS surface compared to the smooth surface observed in AFGNS (Fig. 4b and d). The interlayer spacing of the P-AFGNS was found to be 4.1 Å, similar to that for the AFGNS (Fig. S9b; ESI†). AFM analysis (Fig. S10a; ESI†) shows a thickness of 8.5 nm in P-AFGNS, the increase in comparison to AFGNS being due to the polymer encapsulation. But the size of the nanosheets did not change noticeably after PEGylation as observed from the TEM (Fig. S9a; ESI†) and AFM images (Fig. S10a and b; ESI†) The FESEM micrographs of AFGNS (Fig. S11a; ESI†) shows graphitic flakes with no polymeric attachment whereas in the case of P-AFGNS (Fig. S11b; ESI†), the presence of the PEG polymer on the surface of AFGNS was clearly visible.

The anticancer drug DOX was loaded on P-AFGNS and AFGNS by a mixing and sonication process. In the case of AFGNS-DOX, the loading capacity from UV-Vis spectra (Fig. S12a; ESI†) and the calibration graph (Fig. S12b; ESI†) was found to be 0.349 mg mg^{-1}. However, as the composite was not water soluble, PEGylation was subsequently carried out on AFGNS–DOX. It is noteworthy here that during PEGylation, ultrasonic treatment is necessary for about 60 min. As the DOX is loaded on AFGNS primarily by weak π−π stacking interaction,[34] during the ultrasonic treatment, the interaction between DOX and AFGNS was weakened leading to the detachment of DOX from the AFGNS surface. The supernatant water after ultrasonication turned red and showed a strong peak of DOX due to its detachment. This method was thus not found to be feasible. Alternatively, carrying out PEGylation of AFGNS *via* covalent bonding and subsequent DOX loading was found to overcome the previously mentioned problems and a water-soluble P-AFGNS−DOX composite was successfully prepared. The evidence of successful loading of DOX in P-AFGNS was observed from the FTIR spectra of P-AFGNS, P-AFGNS-DOX and DOX as shown in Fig. 6a. In the case of P-AFGNS-DOX, the powder was washed several times with distilled water to remove any unbound DOX present on the surface of the sample. Presence of peaks at 870 cm^{-1} for C–H bending, 1204 and 1278 cm^{-1} for C–O stretching and the prominent peak at 1417 cm^{-1} for C–C stretching of DOX[46] in the spectra of P-AFGNS−DOX (Fig. 6a) confirmed the presence of DOX on the P-AFGNS surface. Further, appearance of a relatively broad peak in the O–H stretching region (near 3437 cm^{-1}) is expected to be due to the hydrogen bonding interaction of DOX and P-AFGNS originated –OH groups.[33] The drug loading capacity of P-AFGNS (Fig. S12c; ESI†) was calculated to be 0.296 mg mg^{-1} which is slightly different than AFGNS. It is clear that DOX is loaded on AFGNS mainly *via* π–π stacking interaction, whereas, in the case of P-AFGNS, H-bonding between the DOX originated groups with PEG as well as some π–π interaction with the nanosheets were expected to occur.[33] So, the loading capacity in the two cases can be different. It is noteworthy here that the P-AFGNS-DOX composite has high solubility in water and the drug loading capacity in this case is higher than the drug loading capacity of other common drug carrier materials such as liposomes and chitosans which have less than 0.1 mg mg^{-1} drug loading capacity.[60,61]

The drug release study was performed at pH values of 5.5 and 7.4 at 37 °C (*in vivo* physiological temperature) and 25 °C (room temperature) as shown in Fig. 6b. The release of DOX was found to be very low under physiological pH conditions with only about 20.1 and 16.8% of the bound DOX released over 72 h at pH 7.4 at 37 and 25 °C respectively. However, under acidic pH conditions, around 59 and 37.5% of DOX was released over the same period of time at 37 and 25 °C, respectively. Such enhanced release of DOX at lower pH confirms the hydrogen bonding interaction of P-AFGNS with DOX.[62] The photoluminescence emission study of the DOX, released after 72 h (Fig. 6c) shows much lower intensity of the spectra at pH 7.4 compared to pH 5.5 for the supernatant solution containing the dissolved released DOX (when irradiated under a UV lamp of 440 nm wavelength)[63] at both the temperatures. Typically, for the drug delivery processes, the drug is first transported to the tumour cells where it is taken up by endocytosis and finally in the acidic pH of the lysosomes (pH 5.5) present inside the tumour cells, protonation of the $–NH_2$ group on DOX occurs making it more hydrophilic along with simultaneous weakening of the hydrogen bonding interactions between P-AFGNS and DOX, thus leading to its release.[34,63] Thus, the pH sensitive and sustained release of DOX from the P-AFGNS−DOX composite makes it a highly suitable and potential drug carrier for targeted anticancer drug delivery.

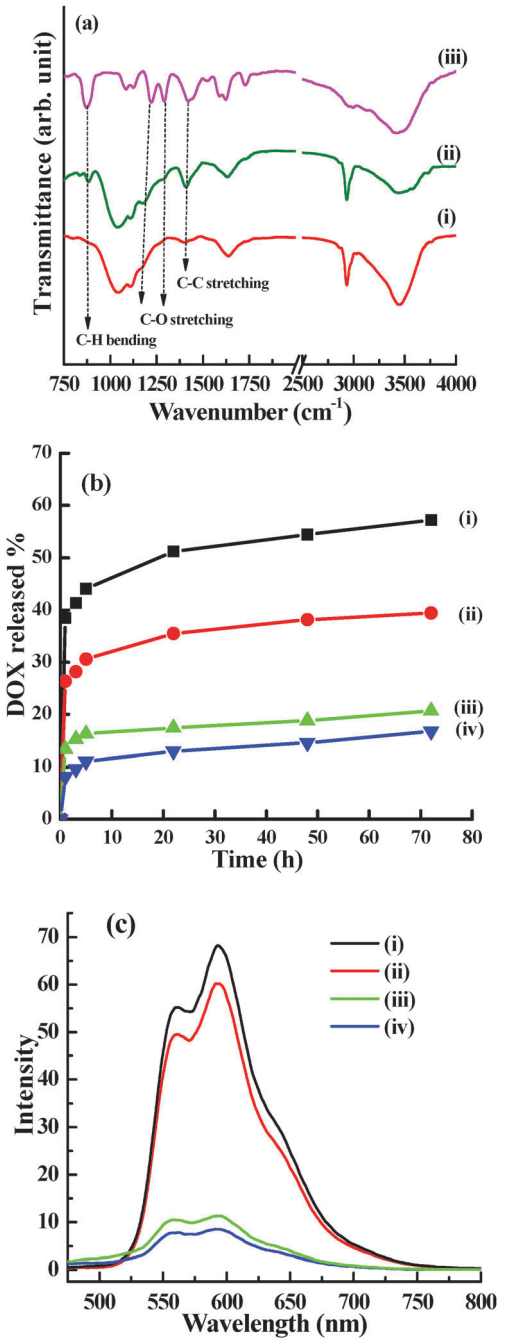

Fig. 6 (a) FTIR spectra of (i) P-AFGNS, (ii) P-AFGNS–DOX and (iii) DOX. (b) Release of DOX from P-AFGNS–DOX and (c) the photoluminescence emission spectra of the supernatant solution containing dissolved DOX after 72 h in (i) pH 5.5 at 37 °C, (ii) pH 5.5 at 25 °C, (iii) pH 7.4 at 37 °C and (iv) pH 7.4 at 25 °C.

Conclusion

A cost effective, easy and efficient route towards the synthesis of a $-NH_2$ functionalized graphite nanosheet is described. The process involves two simple steps of chemical functionalization involving nitration followed by reduction. The $-NH_2$ derivatized graphite nanosheets were further functionalized with –COOH terminated polyethylene glycol chains to form a water-soluble graphite nanosheet composite which is expected to be much less cytotoxic in nature compared to some of its oxide counterparts. The anticancer drug doxorubicin was loaded on to this nanosheet composite with a sufficient loading capacity of 0.296 mg mg^{-1} and its release from this composite was monitored at pH 5.5 and 7.4 over 72 h at 25 and 37 °C. The cost effective, efficient and sustained drug release of up to 59% in pH 5.5 at 37 °C (pH of the tumour cell and body temperature respectively) over 72 h makes it a potential drug carrier for applications in the field of targeted drug delivery.

Notes and references

1 H. Dai, Z. Liu, X. Li and X. Sun, *US Pat.*, 8535726 B2, 2013.
2 W. S. Seo, J. H. Lee, X. Sun, Y. Suzuki, D. Mann, Z. Liu, M. Terashima, P. C. Yang, M. V. McConnell, D. G. Nishimura and H. Dai, *Nat. Mater.*, 2006, **5**, 971.
3 L. Wang, G. Mu, C. Tian, L. Sun, W. Zhou, T. Tan and H. Fu, *ChemSusChem*, 2012, **5**(12), 2442.
4 H. Ji, D. P. Sellan, M. T. Pettes, X. Kong, J. Ji, L. Shi and R. S. Ruoff, *Energy Environ. Sci.*, 2014, **7**, 1185.
5 B. R. S. Lemos, I. F. Teixeira, B. F. Machado, M. R. A. Alves, J. P. de Mesquita, R. R. Ribeiro, R. R. Bacsa, P. Serp and R. M. Lago, *J. Mater. Chem. A*, 2013, **1**, 9491.
6 A. Bianco, H. M. Cheng, T. Enoki, Y. Gogotsi, R. H. Hurt, N. Koratkar, T. Kyotani, M. Monthioux, C. R. Park, J. M. D. Tascon and J. Zhang, *Carbon*, 2013, **65**, 1.
7 A. Mukherjee, J. H. Kang, O. Kuznetsov, Y. Sun, R. Thaner, A. S. Bratt, J. R. Lomeda, K. F. Kelly and W. E. Billups, *Chem. Mater.*, 2011, **23**(1), 9.
8 J. Chattopadhyay, A. Mukherjee, S. Chakraborty, J. H. Kang, P. J. Loos, K. F. Kelly, H. K. Schmidt and W. E. Billups, *Carbon*, 2009, **47**(13), 2945.
9 B. Standley, A. Mendez, E. Schmidgall and M. Bockrath, *Nano Lett.*, 2012, **12**(3), 1165.
10 H. Shen, M. Liu, H. He, L. Zhang, J. Huang, Y. Chong, J. Dai and Z. Zhang, *ACS Appl. Mater. Interfaces*, 2012, **4**, 6317.
11 Z. Liu, J. T. Robinson, X. Sun and H. Dai, *J. Am. Chem. Soc.*, 2008, **130**, 10876.
12 B. Tian, C. Wang, S. Zhang, L. Feng and Z. Liu, *ACS Nano*, 2011, **5**, 7000.
13 X. Ma, H. Tao, K. Yang, L. Feng, L. Cheng, X. Shi, Y. Li, L. Guo and Z. Liu, *Nano Res.*, 2012, **5**, 199.
14 X. Sun, Z. Liu, K. Welsher, J. T. Robinson, A. Goodwin, S. Zaric and H. Dai, *Nano Res.*, 2008, **1**, 203.
15 B. J. Hong, O. C. Compton, Z. An, I. Eryazici and S. T. Nguyen, *ACS Nano*, 2012, **6**, 63.
16 S. Das, S. Singh, V. Singh, D. Joung, J. M. Dowding, D. Reid, J. Anderson, L. Zhai, S. I. Khondaker, W. T. Self and S. Seal, *Part. Part. Syst. Charact.*, 2013, **30**, 148.
17 K. H. Liao, Y. S. Lin, C. W. Macosko and C. L. Haynes, *ACS Appl. Mater. Interfaces*, 2011, **3**, 2607.
18 A. B. Seabra, A. J. Paula, R. Lima, O. L. Alves and N. Duran, *Chem. Res. Toxicol.*, 2014, **27**, 159.

19 S. K. Singh, M. K. Singh, M. K. Nayak, S. Kumari, S. Shrivastava, J. J. A. Grácio and D. Dash, *ACS Nano*, 2011, **5**, 4987.
20 S. K. Singh, M. K. Singh, P. P. Kulkarni, V. K. Sonkar, J. J. A. Grácio and D. Dash, *ACS Nano*, 2012, **6**(3), 2731.
21 Y. Hu, J. Shen, N. Li, M. Shi, H. Ma, B. Yan, W. Wang, W. Huang and M. Ye, *Polym. Compos.*, 2010, **31**, 1987.
22 M. Guo, D. Li, M. Zhao, Y. Zhang, D. Geng, A. Lushington and X. Sun, *Carbon*, 2013, **61**, 321.
23 M. Guo, M. Li, X. Liu, M. Zhao, D. Li, D. Geng, X. Sun and H. Gu, *J. Mater. Sci.: Mater. Med.*, 2013, **24**, 2741.
24 H. Wu, H. Shi, Y. Wang, X. Jia, C. Tang, J. Zhang and S. Yang, *Carbon*, 2014, **69**, 379.
25 Y. C. Lin, C. Y. Lin and P. W. Chiu, *Appl. Phys. Lett.*, 2010, **96**, 133110.
26 N. H. Kim, T. Kuila and J. H. Lee, *J. Mater. Chem. A*, 2013, **1**, 1349.
27 M. Quintana, K. Spyrou, M. Grzelczak, W. R. Browne, P. Rudolf and M. Prato, *ACS Nano*, 2010, **4**, 3527.
28 P. L. Girard-Lauriault, R. Illgen, J. C. Ruiz, M. R. Wertheimer and W. E. S. Unger, *Appl. Surf. Sci.*, 2012, **258**, 8448.
29 E. Yang and M. Nagatsu, *Jpn. J. Appl. Phys.*, 2014, **53**, 010206.
30 Y. Geng, J. Li, S. J. Wang and J. K. Kim, *J. Nanosci. Nanotechnol.*, 2008, **8**(12), 6238.
31 J. Chattopadhyay, F. J. Cortez, S. Chakraborty, N. K. H. Slater and W. E. Billups, *Chem. Mater.*, 2006, **18**, 5864.
32 L. E. Vlerken, T. K. Vyas and M. M. Amiji, *Pharm. Res.*, 2007, **24**, 1405.
33 R. Kurapatia and A. M. Raichur, *Chem. Commun.*, 2012, **48**, 6013.
34 X. Yang, Y. Wang, X. Huang, Y. Ma, Y. Huang, R. Yang, H. Duan and Y. Chen, *J. Mater. Chem.*, 2011, **21**, 3448.
35 K. Schofield, *Aromatic nitration*, Cambridge University Press, 1980.
36 G. A. Olah, S. J. Kuhn, S. H. Flood and J. C. Evans, *J. Am. Chem. Soc.*, 1962, **84**, 3687.
37 D. E. Nixon, G. S. Parry and A. R. Ubbelohde, *Proc. R. Soc. A*, 1966, **291**, 324.
38 W. C. Forsman, F. L. Vogel, D. E. Carl and J. Hoffman, *Carbon*, 1978, **16**(4), 269–271.
39 S. Park and R. S. Ruoff, *Nat. Nanotechnol.*, 2009, **4**, 217.
40 C. Xin-Yun, *Int. Nano Lett.*, 2013, **3**, 6.
41 D. Huber, G. Andermann and G. Leclerc, *Tetrahedron Lett.*, 1988, **29**(6), 635.
42 G. W. Kabalka and R. S. Verma, *Reduction of nitro and nitroso compounds*, Pergamon press, Oxford, UK, vol. 8, 1991.
43 S. K. Maity, N. C. Pradhan and A. V. Patwardhan, *Appl. Catal., A*, 2006, **301**(2), 251.
44 K. Bhowmik, S. Pramanik, S. K. Medda and G. De, *J. Mater. Chem.*, 2012, **22**, 24690.
45 V. Georgakilas, A. B. Bourlinos, R. Zboril, T. A. Steriotis, P. Dallas, A. K. Stubos and C. Trapalis, *Chem. Commun.*, 2010, **46**, 1766.
46 W. Kemp, *Organic Spectroscopy*, Palgrave, New York, 3rd edn, 1991.
47 H. Kitamura, M. Sekido, H. Takeuchi and M. Ohno, *Carbon*, 2011, **49**, 3851.
48 T. Ramanathan, F. T. Fisher, R. S. Ruoff and L. C. Brinson, *Chem. Mater.*, 2005, **17**, 1290.
49 A. Mukherjee, R. Combs, J. Chattopadhyay, D. W. Abmayr, P. S. Engels and W. E. Billups, *Chem. Mater.*, 2008, **20**, 7339.
50 H. Sun, N. Gao, L. Wu, J. Ren, W. Wei and X. Qu, *Chem. – Eur. J.*, 2013, **19**, 13362.
51 T. I. T. Okpalugo, P. Papakonstantinou, H. Murphy, J. McLaughlin and N. M. D. Brown, *Carbon*, 2005, **43**, 153.
52 C. Moreno-Castilla, M. V. López-Ramón and F. Carrasco-Maŕın, *Carbon*, 2000, **38**, 1995.
53 W. Xia, Y. Wang, R. Bergsträßer, S. Kundu and M. Muhler, *Appl. Surf. Sci.*, 2007, **254**, 247.
54 Y. Zhu, A. L. Higginbotham and J. M. Tour, *Chem. Mater.*, 2009, **21**, 5284.
55 V. C. Sanchez, A. Jachak, R. H. Hurt and A. B. Kane, *Chem. Res. Toxicol.*, 2012, **25**, 15.
56 Y. Wang, Z. Li, D. Hu, C. Lin, J. Li and Y. Lin, *J. Am. Chem. Soc.*, 2010, **132**, 9274.
57 C. Lu, C. Zhu, J. Li, J. Liu, X. Chen and H. Yang, *Chem. Commun.*, 2010, **46**, 3116.
58 X. Zhao, L. Liu, X. Li, J. Zeng, X. Jia and P. Liu, *Langmuir*, 2014, **30**, 10419.
59 L. Zhang, Z. Wang, Z. Lu, H. Shen, J. Huang, Q. Zhao, M. Liu, N. He and Z. Zhang, *J. Mater. Chem. B*, 2013, **1**, 749.
60 W. T. Sun, N. Zhang, A. G. Li, W. W. Zou and W. F. Xu, *Int. J. Pharm.*, 2008, **353**, 243.
61 E. K. Lim, W. Sajomsang, Y. Choi, E. Jang, H. Lee, B. Kang, E. Kim, S. Haam, J. S. Suh, S. J. Chung and Y. M. Huh, *Nanoscale Res. Lett.*, 2013, **8**, 467.
62 C. Tapeinos, E. K. Efthimiadou, N. Boukos, C. A. Charitidis, M. Koklioti and G. Kordas, *J. Mater. Chem. B*, 2013, **1**, 194.
63 C. W. Lai, Y. H. Hsiao, Y. K. Peng and P. T. Chou, *J. Mater. Chem.*, 2012, **22**, 14403.

